

Supplementary information to

Chemoselective guest-triggered shaping of a polynuclear Cu^{II} calix[6]complex into a molecular host.

Sarah Richard, Gaëtan Le Duc, Nicolas Le Poul, Yves Le Mest, Olivia Reinaud and Jean-Noël Rebilly

Materials and methods. Solvents and chemicals were of reagent grade and were used without purification. HR-MS were performed at the Institut de Chimie des Substances Naturelles, Gif-sur-Yvette, France. ESI-MS analyses were obtained with a ThermoFinnigen LCQ Advantage spectrometer using methanol and dichloromethane as solvents. NMR spectra were recorded on a Bruker ARX250 MHz spectrometer or an Advance 500 spectrometer. EPR spectra were recorded using a Bruker Elexys spectrometer (X-band). The electrochemical studies of the copper complexes have been performed in a glovebox (Jacomex) ($O_2 < 1\text{ ppm}$, $H_2O < 1\text{ ppm}$) with a home-designed 3-electrode cell (WE, GC; RE, Pt in Fc^+/Fc solution; CE, Pt). The potential of the cell was controlled by an AUTOLAB PGSTAT 100 (Ecochemie) potentiostat monitored by a computer. UV-vis-NIR spectroscopy was performed with a JASCO V-670 spectrophotometer.

Table des matières

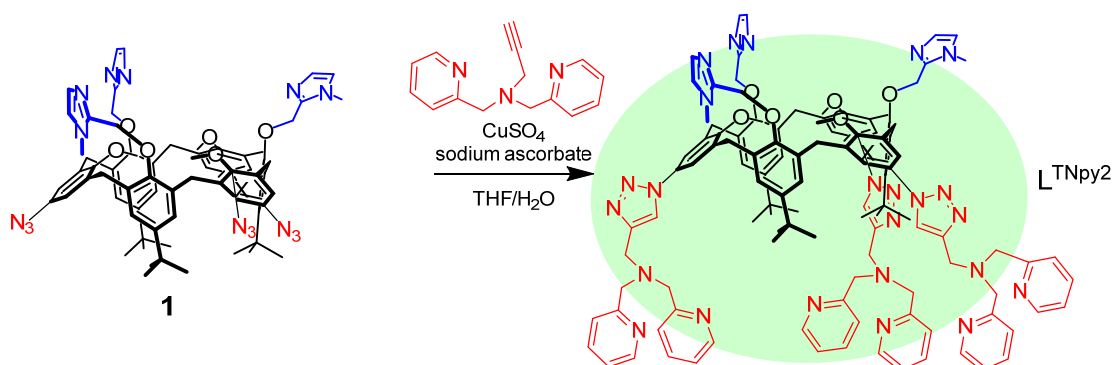
I/ Synthesis of the tetradentate system L^{TNpy2}	2
II/ Coordination and host-guest studies on the small rim reference ligand L^{tBu}	5
2.1. EPR studies of the Cu ^{II} complexes of reference small rim ligand L^{tBu}	6
2.1.1. $L^{tBu}Cu(S)_2^{2+}$ in MeCN/DMF	6
2.1.2. $L^{tBu}Cu(S)_2^{2+}$ + heptylamine	6
2.2. UV-vis studies of $L^{tBu}Cu(S)^{2+}$ upon addition of heptylamine.....	7
2.3. Electrochemical studies of $L^{tBu}Cu(S)^{2+}$ upon addition of heptylamine	7
III/ Coordination and host-guest studies on the large rim reference tetradentate ligand F^{TNpy2}	8
3.1. EPR studies of Fragment $F^{TNpy2}Cu(S)^{2+}$	8
3.2. EPR studies of Fragment $F^{TNpy2}Cu(S)^{2+} + 2Melm$	8
3.3. EPR studies of Fragment $(F^{TNpy2})_2Cu^{2+}$	9
3.4. EPR studies of Fragment $F^{TNpy2}Cu(S)^{2+} + 2$ heptylamine	9
3.5. UV-vis titration of F^{TNpy2} by Cu ^{II}	11
3.6. Electrochemical titration of F^{TNpy2} by Cu ^{II}	11
3.7. UV-vis titration of $F^{TNpy2} Cu(S)^{2+}$ by heptylamine	12
3.8. Electrochemical titration of $F^{TNpy2} Cu(S)^{2+}$ by heptylamine	12
3.9. Electrochemical titration of $F^{TNpy2} Cu(S)^{2+}$ by N-methylimidazole and tetrabutylammonium hydroxide.....	13
3.10. Discussion: coordination behavior of $F^{TNpy2} Cu^{II}$ complexes	13
IV/ Coordination studies on ligand L^{TNpy2}	15

4.1.	EPR studies of the Cu ^{II} complexes of ligand L ^{TNpy2}	15
4.1.1.	L ^{TNpy2} + 3 equiv. Cu ^{II} in MeCN/DMF	15
4.1.2.	Addition of heptylamine to a mixture of L ^{TNpy2} and 4 equiv. Cu ^{II} in MeCN/DMF	16
4.2.	¹ H NMR coordination and host-guest studies of ligand L ^{TNpy2} towards Zn ^{II}	19
4.2.1.	Addition of Zn ^{II} to L ^{TNpy2} in CD ₃ CN	19
4.2.2.	Addition of heptylamine to a L ^{TNpy2} :Zn ^{II} (1:4) mixture in CD ₃ CN	20
V/	Titrations of free Cu ²⁺ by heptylamine	21
5.1.	EPR studies of free Cu ²⁺ in the presence of heptylamine.....	21
5.2.	UV-vis studies of free Cu ²⁺ in the presence of heptylamine	22
5.3.	Electrochemical studies of free Cu ²⁺ in the presence of heptylamine	22
5.4.	ESI-MS studies of the polynuclear L ^{TNpy2} /Cu ²⁺ systems	23

I/ Synthesis of the tetradentate system L^{TNpy2}

Calixarene ligands **1** and L^{TNpy2} were synthesized according to a previously reported procedure.^{1,2} N,N-bis(pyridin-2-ylmethyl)prop-2-yn-1-amine was synthesized according to literature procedures.³

Synthesis of L^{TNpy2}



To a mixture of calixarene **1** (50 mg, 40 μ mol), N,N-bis(pyridin-2-ylmethyl)propargylamine (33 mg, 139 μ mol), sodium ascorbate (57 mg, 287 μ mol) and CuSO₄·5H₂O (36 mg, 142 μ mol) were added 300 μ L of H₂O and 2 mL of THF under argon in a screw cap tube. The reaction mixture was stirred at 60°C for 24 hours. The residue was diluted with THF (20 mL) and water (5 mL) and 10 drops of concentrated ammonia were added. Ethylenediamine tetraacetic acid bis sodium salt (200 mg, excess) was added and the mixture was stirred in air overnight. THF was evaporated and the aqueous phases extracted with CH₂Cl₂ (3 x 10 mL). The organic extracts were combined and washed with brine (5 mL), dried over Na₂SO₄, filtered and concentrated. The brown solid was washed with diethylether (2 x 4 mL) and dried under vacuum (65.3 mg, 83%).

^1H (500 MHz, CD_3CN , 340 K) δ (ppm): 1.03 (s, 27H, *t*Bu), 2.90 (s, 9H, OMe), 3.40 (s, 9H, NMeIm), 3.86 (m, 30H, CH_2py + CH_2Tria + CH_2Ar), 4.79 (s, 6H, CH_2Im), 6.84 (m, 6H, HIm), 6.96 (s, 6H, H_{Ar}*t*Bu), 7.12 (m, 6H, H_{py}(meta)), 7.48 (s, 6H, H_{Ar}Tria), 7.54 (m, 6H, H_{py}(meta')), 7.64 (m, 3H, H_{py}(para)), 7.94 (m, 3H, H_{Tria}), 8.46 (m, 3H, H_{py}(ortho)). **^{13}C (125 MHz, CD_3CN , 300 K)** δ (ppm): 161.10, 157.95, 153.95, 150.16, 149.93, 148.16, 146.82, 145.48, 137.41, 134.70, 134.13, 128.74, 126.86, 124.28, 123.76, 123.13, 122.93, 68.12, 61.49, 61.14, 50.26, 35.16, 33.57, 32.09, 31.88.

ESI-MS (CH_3CN) m/z : 1964.9 (calc. 1965.0 for $[\text{L}^{\text{TNpy}2}+\text{H}]^+$), 982.8 (calc. 983.0 for $[\text{L}^{\text{TNpy}2}+2\text{H}]^{2+}$), 1013.2 (calc. 1013.4 for $[\text{L}^{\text{TNpy}2}+\text{Cu}]^{2+}$), 655.7 (calc. 655.7 for $[\text{L}^{\text{TNpy}2}+3\text{H}]^{3+}$).

HR-MS the main peak ($m/z = 982.5266$) is associated to mass 1965.0532 (charge +2) and corresponds to the formula $\text{C}_{117}\text{H}_{128}\text{N}_{24}\text{O}_6$ in agreement with $[\text{L}^{\text{TNp}2y} + 2\text{H}]^{2+}$ (mass error: 4.2 ppm).

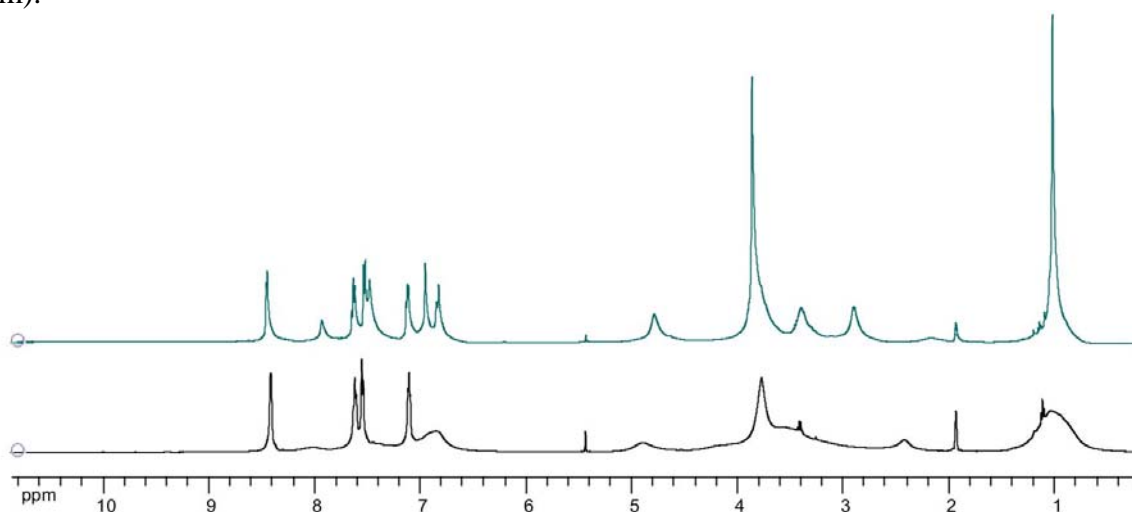


Figure S1. ^1H NMR spectra (500 MHz, CD_3CN) of $\text{L}^{\text{TNPy}2}$ at 300 K (black) and 340 K (blue).

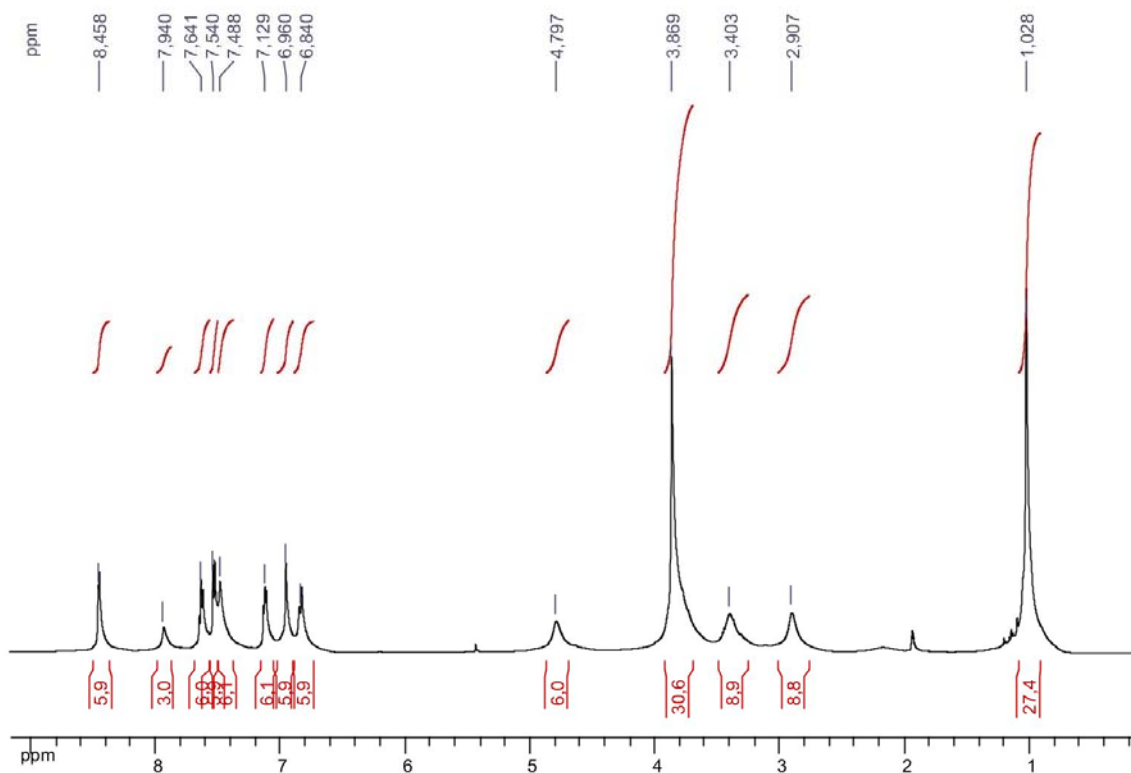


Figure S2. ^1H NMR spectrum of $L^{\text{TNpy}2}$ (500 MHz, CD_3CN , 340K)

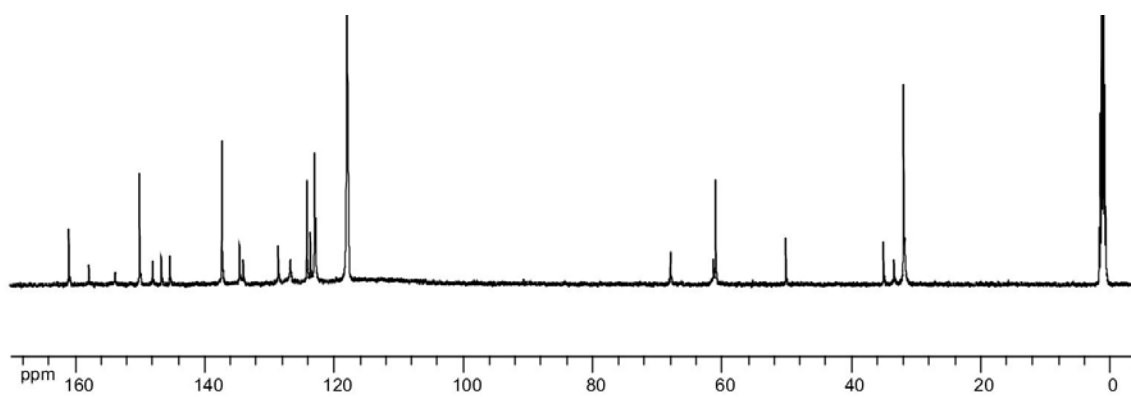


Figure S3. ^{13}C NMR spectrum of $L^{\text{TNpy}2}$ (125 MHz, CD_3CN , 340K)

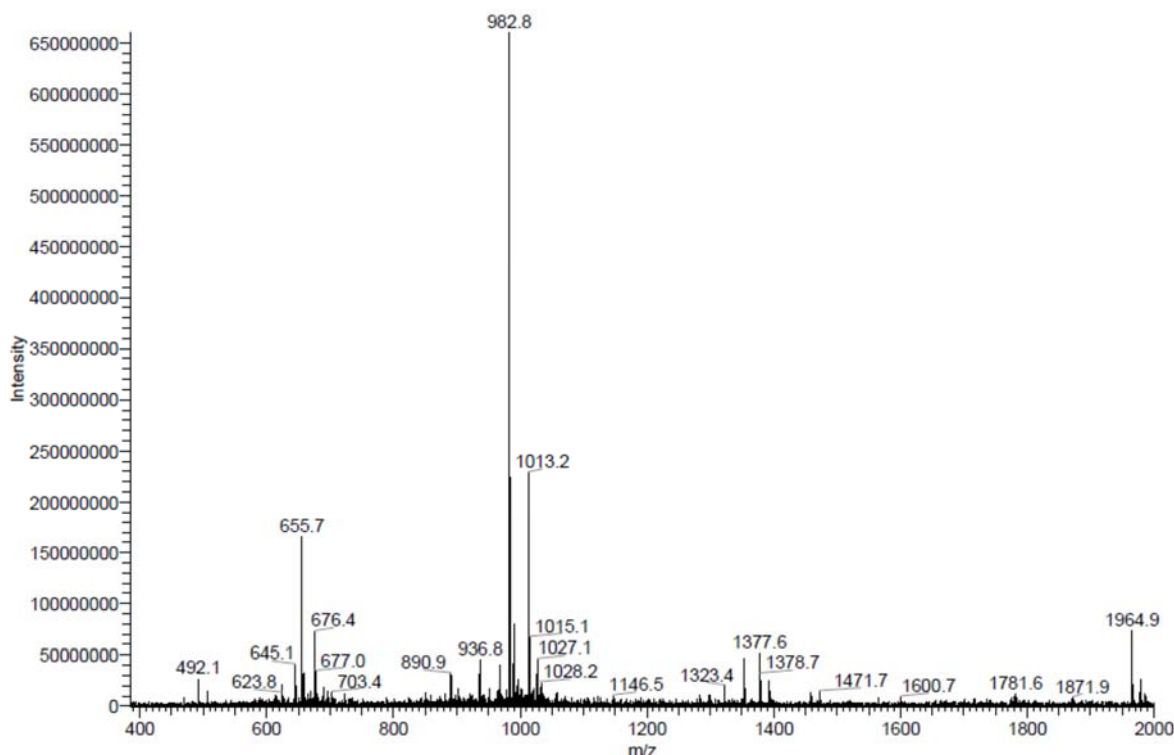


Figure S4. ESI-MS (MeCN) spectrum of L^{TNpy2} .
 CH_3CN m/z : 1964.9 (calc. 1965.0 for $[L^{TNpy2}+H]^+$), 982.8 (calc. 983.0 for $[L^{TNpy2}+2H]^{2+}$),
 1013.2 (calc. 1013.4 for $[L^{TNpy2}+Cu]^{2+}$), 655.7 (calc. 655.7 for $[L^{TNpy2}+3H]^{3+}$).

Elemental Composition Report

Page 1

Single Mass Analysis

Tolerance = 5.0 PPM / DBE: min = -1.5, max = 80.0

Element prediction: Off

Number of isotope peaks used for i-FIT = 3

Monoisotopic Mass, Odd and Even Electron Ions

1 formula(e) evaluated with 1 results within limits (up to 50 closest results for each mass)

Elements Used:

C: 110-117 H: 110-130 N: 19-24 O: 4-6

X6-TPA3-468

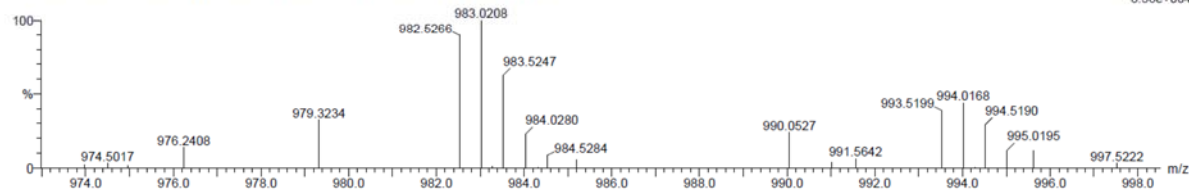
UMR8601_X6-TPA3-468 15 (0.403) AM (Cen,8, 80.00, Ar,5500.0,556.28,0.70,LS,20), Cm (14:29)

LCT

15-Nov-2010 17:19:09

1: TOF MS ES+

8.56e+004



Minimum:

200.0 5.0 -1.5

Maximum:

80.0

Mass	Calc. Mass	mDa	PPM	DBE	i-FIT	i-FIT (Norm)	Formula
1965.0532	1965.0449	8.3	4.2	66.0	-1.5	n/a	C117 H128 N24 O6

1965.0532 1965.0449 8.3 4.2 66.0 -1.5 n/a C117 H128 N24 O6

Figure S5. HR-MS (MeCN) spectrum of L^{TNpy2} .

The main peak ($m/z = 982.5266$) is associated to mass 1965.0532 (charge +2) and corresponds to the formula $C_{117}H_{128}N_{24}O_6$ in agreement with $[L^{TNpy2} + 2H]^{2+}$ (mass error: 4.2 ppm).

II/ Coordination and host-guest studies on the small rim reference ligand L^{tBu}

2.1. EPR studies of the Cu^{II} complexes of reference small rim ligand L^{tBu}

2.1.1. L^{tBu}Cu(S)₂²⁺ in MeCN/DMF

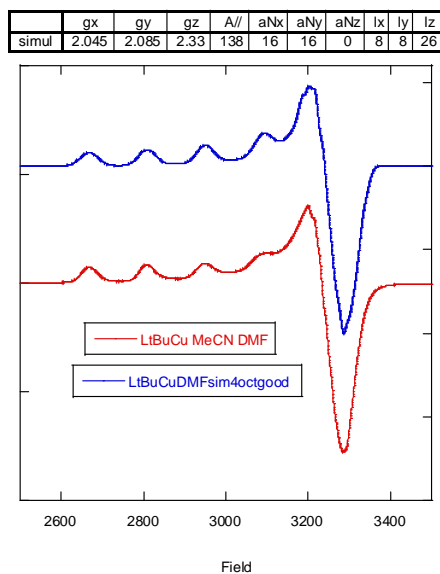


Figure S6. X band EPR spectra (100 K) of LtBuCu²⁺ (6 mM in MeCN/DMF 1:1) and corresponding simulation. A// and a_N values in G.

2.1.2. L^{tBu}Cu(S)₂²⁺ + heptylamine

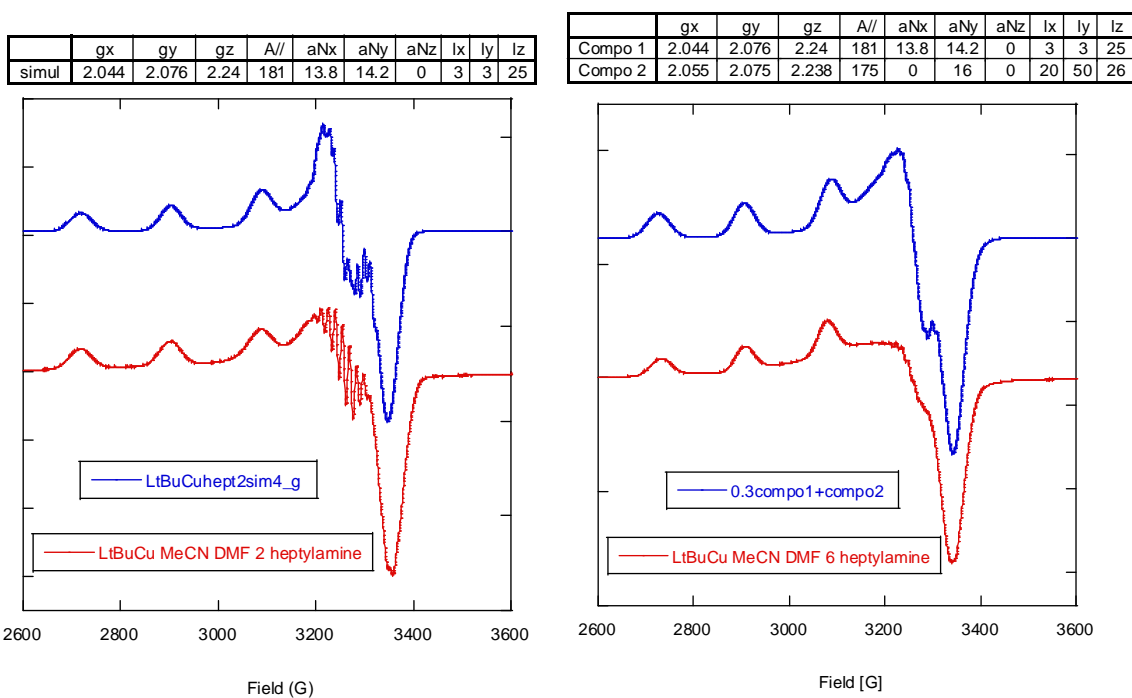


Figure S7. X band EPR spectra (100 K) of LtBuCu(S)₂²⁺ (6 mM in MeCN/DMF 1:1) in the presence of 2 (left) and 6 (right) equiv. heptylamine, and corresponding simulation. A// and a_N values in G.

2.2. UV-vis studies of $L^{tBu}Cu(S)^{2+}$ upon addition of heptylamine

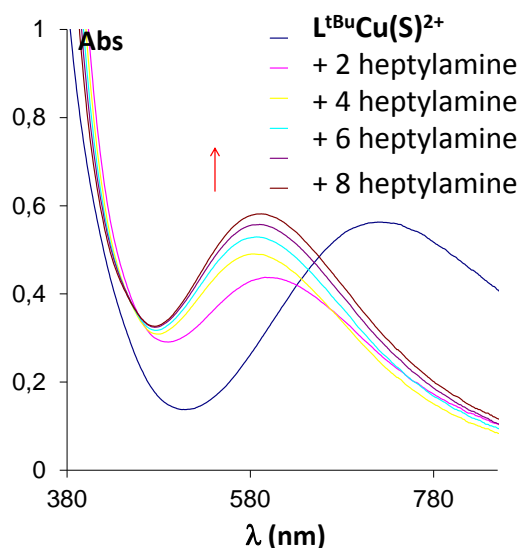


Figure S8. Evolution of the UV-vis spectra upon addition of heptylamine to a) a 1 :1 mixture of L^{tBu} and $Cu^{II}(OTf)_2$ in MeCN/DMF 1 :1 . The absorption maximum shifts in two steps: 605 nm, then from 605 to 590 nm upon heptylamine binding.

2.3. Electrochemical studies of $L^{tBu}Cu(S)^{2+}$ upon addition of heptylamine

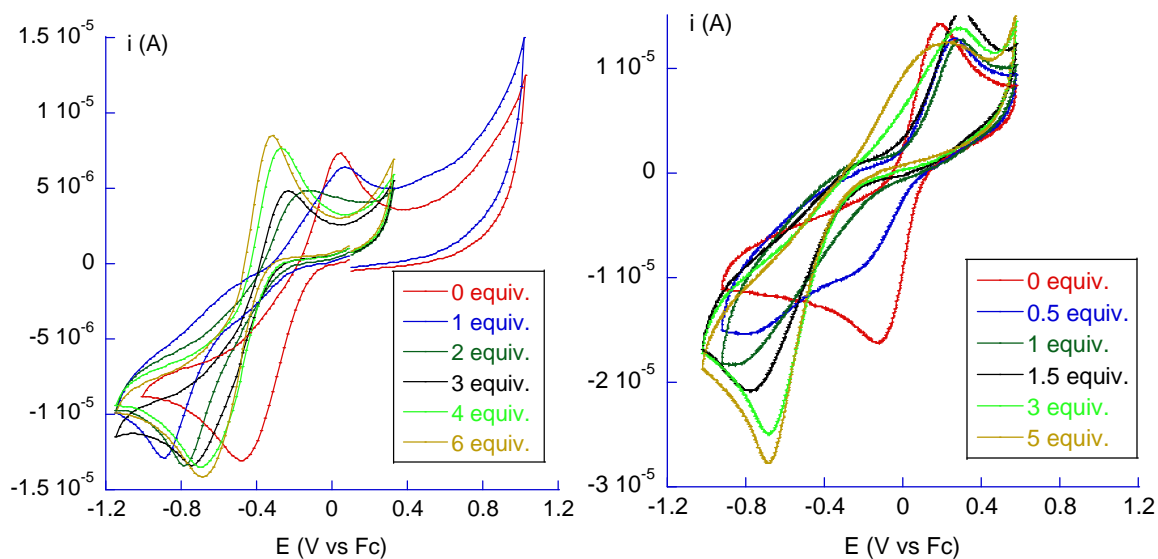


Figure S9. Cyclic voltammograms recorded during the addition of heptylamine to the $L^{tBu}Cu(S)_2^{2+}$. NBu_4PF_6 0.1 M in MeCN/DMF 1:1 (left, ClO_4^- salt) and MeCN (right, OTf^- salt) (CE: Pt, Ref: Fc^+/Fc , 0.5 V/s). WE: GC.

III/ Coordination and host-guest studies on the large rim reference tetradentate ligand F^{TNpy2}

3.1. EPR studies of Fragment $F^{TNpy2}Cu(S)^{2+}$

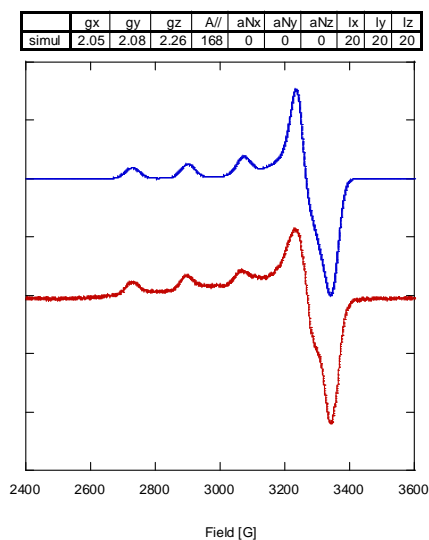


Figure S10. X band EPR spectra (100 K) of a mixture of F^{TNpy2} and 1 equiv. Cu^{2+} (6 mM in MeCN/DMF 1:1, red) and corresponding simulation (blue). $A_{//}$ and a_N values in G.

3.2. EPR studies of Fragment $F^{TNpy2}Cu(S)^{2+} + 2Melm$

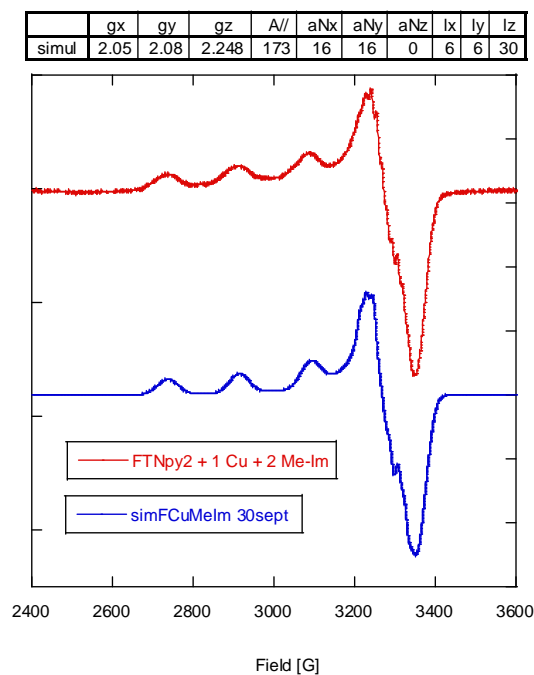


Figure S11. X band EPR spectra (100 K) of a mixture of F^{TNpy2} , 1 equiv. Cu^{2+} and 1 equiv. 2-methylimidazole (6 mM in MeCN/DMF 1:1) and corresponding simulation. $A_{//}$ and a_N values in G.

3.3. EPR studies of Fragment $(F^{TNpy2})_2Cu^{2+}$

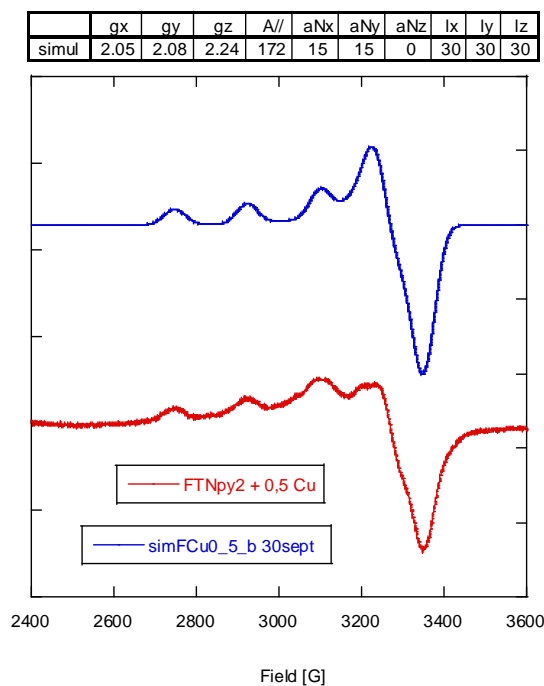


Figure S12. X band EPR spectra (100 K) of a mixture of F^{TNpy2} and 0.5 equiv. Cu^{2+} (6 mM in MeCN/DMF 1:1) and corresponding simulation. $A_{//}$ and a_N values in G.

3.4. EPR studies of Fragment $F^{TNpy2}Cu(S)^{2+} + 2$ heptylamine

The spectrum displays two sets of signals and was simulated as the sum of 2 components.

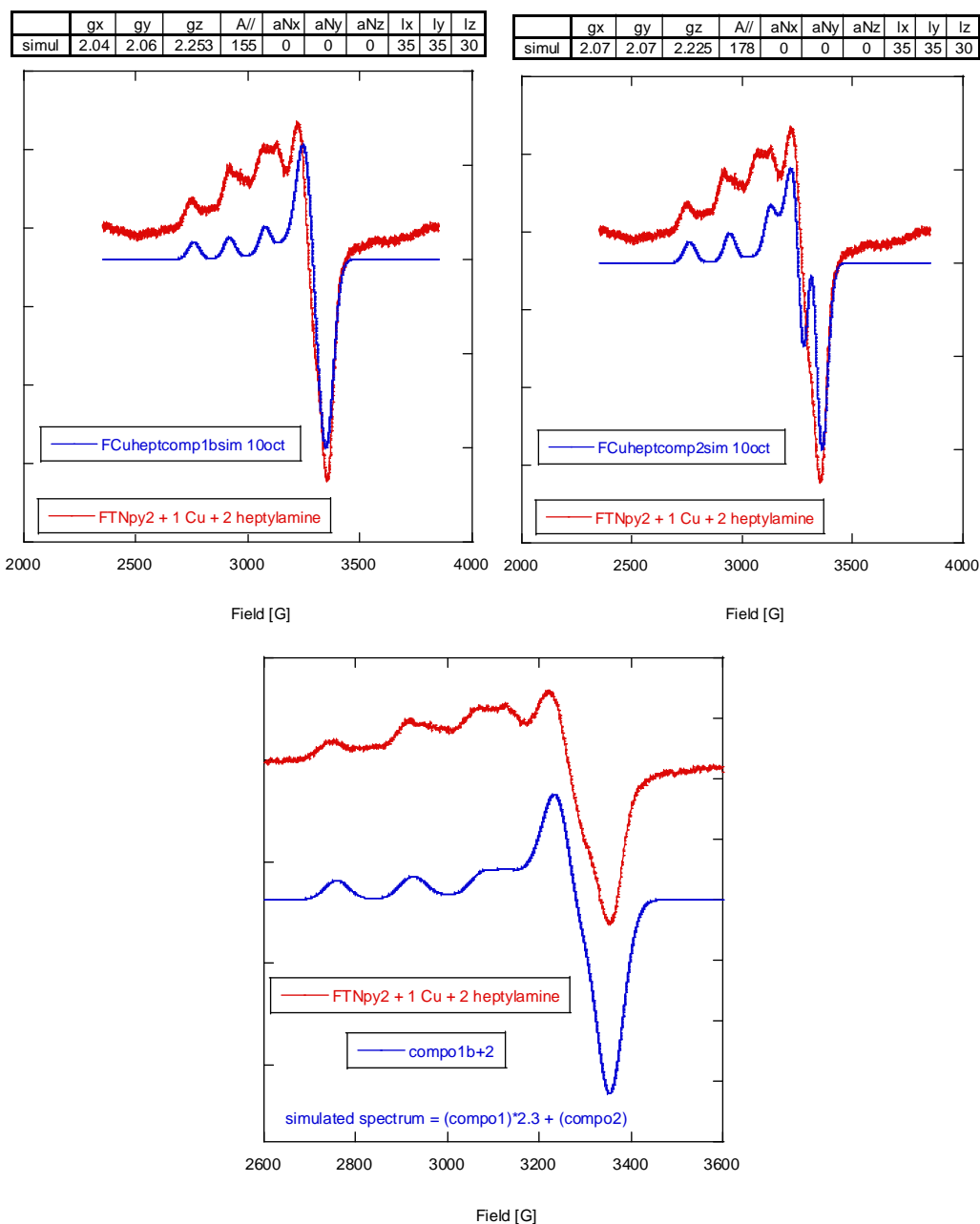


Figure S13. *Top*: X band EPR spectra (100 K) of a mixture of $\text{F}^{\text{TNpy}2}$, 1 equiv. Cu^{2+} and 2 equiv. heptylamine (6 mM in MeCN/DMF 1:1) and corresponding simulations. $A_{//}$ and a_N values in G. The spectrum displays two sets of signals and was simulated as the sum of 2 components. *Top*: isolated components simulations; *Bottom*: sum of the simulated spectra of the two components [$2.3 \times (\text{component 1}) + \text{component 2}$].

3.5. UV-vis titration of F^{TNPpy2} by Cu^{II}

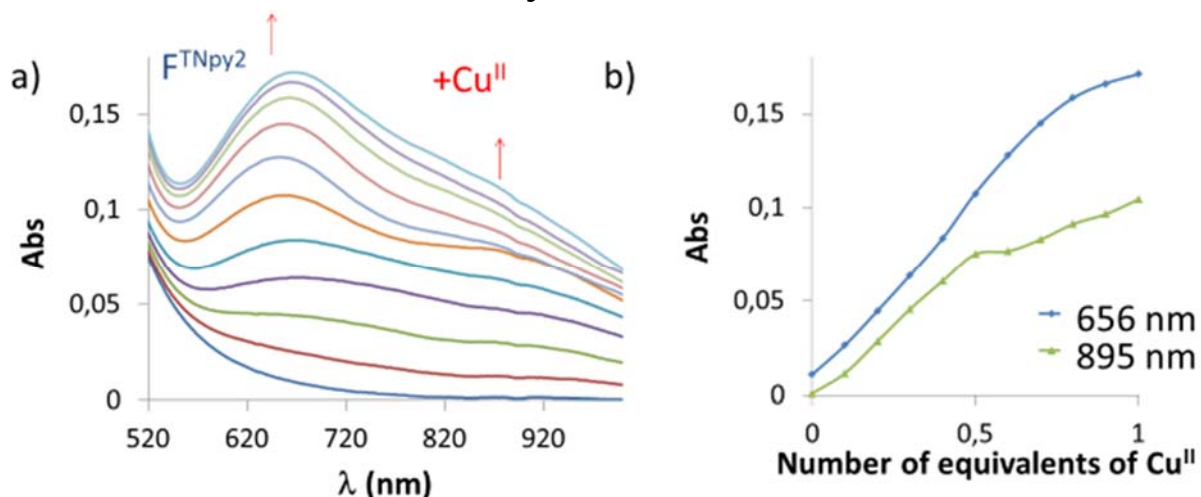


Figure S14. UV-vis titrations of F^{TNPpy2} (2 mM) by $Cu^{II}(OTf)_2$ in MeCN/DMF (a). Successive curves correspond to aliquots of 0.1 equiv. Cu^{II} (for F^{TNPpy2}). Absorbance evolution at 2 wavelengths during the titration (b).

3.6. Electrochemical titration of F^{TNPpy2} by Cu^{II}

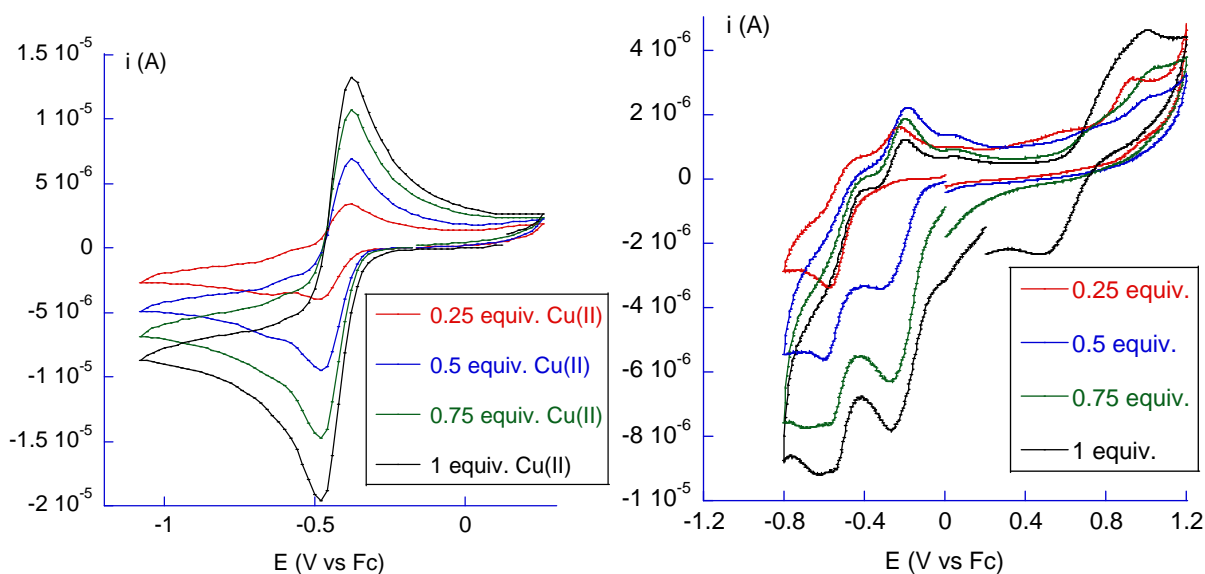


Figure S15. CVs (E/V vs Fc, $v = 0.1$ V/s, NBu_4PF_6 0.1 M) recorded upon addition of Cu^{II} to the ligand F^{TNPpy2} . *Left*: in MeCN/DMF (WE: GC), $Cu(ClO_4)_2$ salt. *Right*: in MeCN (WE: Pt), $Cu(OTf)_2$ salt.

3.7. UV-vis titration of $F^{TNPpy2} Cu(S)^{2+}$ by heptylamine

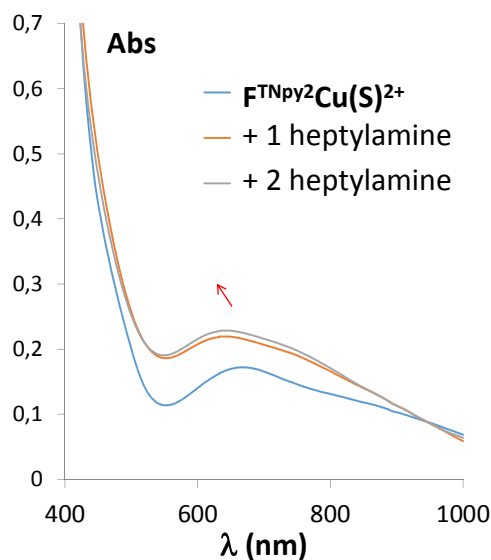


Figure S16. Evolution of the UV-vis spectra upon addition of heptylamine to a) a 1 : 1 mixture of F^{TNPpy2} and $Cu^{II}(OTf)_2$ in MeCN/DMF 1 : 1 .

3.8. Electrochemical titration of $F^{TNPpy2} Cu(S)^{2+}$ by heptylamine

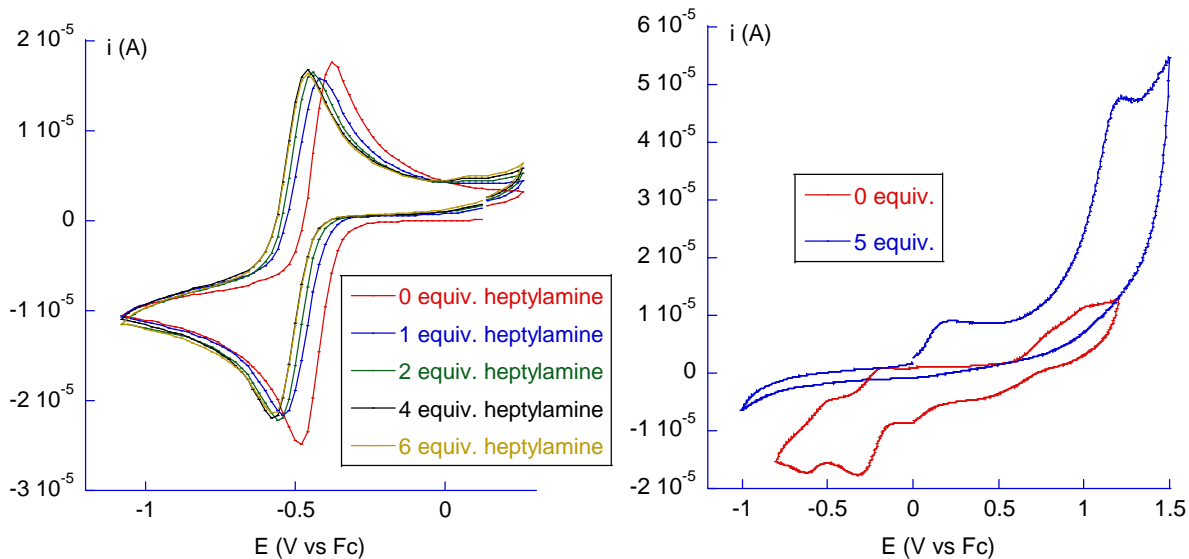


Figure S17. CVs at GC electrode (E/V vs Fc, $v = 0.1$ V/s, NBu_4PF_6 0.1 M) recorded upon addition of heptylamine to a mixture of $F^{TNPpy2+} + 1$ equiv. Cu^{2+} . *Left*: in MeCN/DMF, ClO_4^- salt. *Right*: in MeCN, OTf^- salt. Solutions were scanned in reduction to the lowest possible potential to discard the appearance of a redissolution peak in oxidation.

3.9. Electrochemical titration of $F^{TNpy2} Cu(S)^{2+}$ by N-methylimidazole and tetrabutylammonium hydroxide

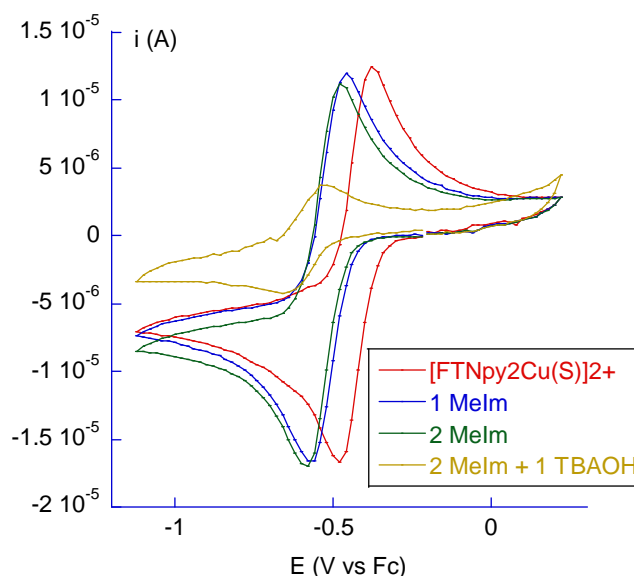


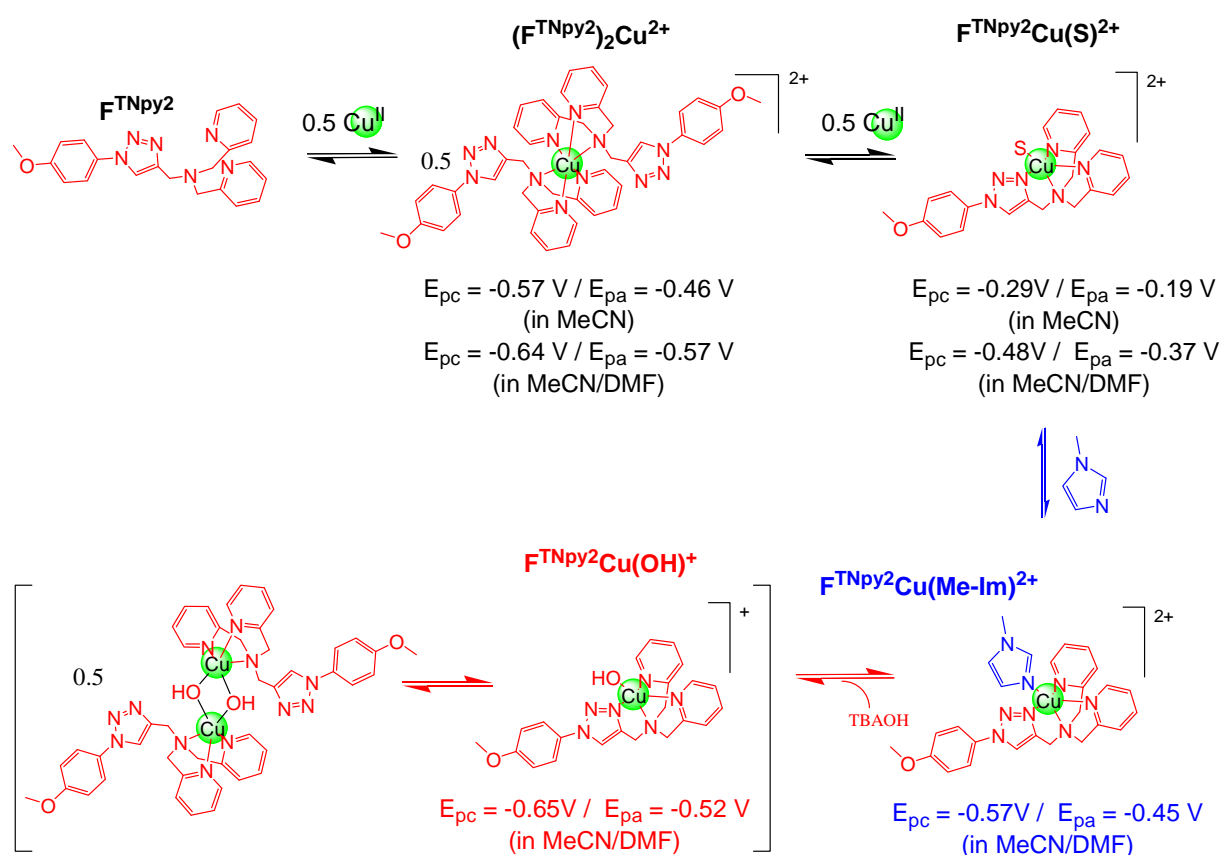
Figure S18. CVs at GC electrode (E/V vs Fc, $v = 0.1$ V/s, NBu_4PF_6 0.1 M) recorded upon addition of N-methylimidazole and tetrabutylammonium hydroxide to a mixture of $F^{TNpy2+} + 1$ equiv. Cu^{2+} (ClO_4^- salt) in MeCN/DMF. Solutions were scanned in reduction to the lowest possible potential to discard the appearance of a redissolution peak in oxidation.

3.10. Discussion: coordination behavior of $F^{TNpy2} Cu^{II}$ complexes

Titration of F^{TNpy2} by Cu^{II} (Figure S14) shows the increase of two bands at 653 and 892 nm between 0 and 0.5 equivalents of Cu^{II} . Between 0.5 and 1 equivalent, the first shifts to 667 nm and becomes predominant over the second one, as can be seen on the absorbance evolution at 656 and 895 nm. This is ascribed to the successive formation of complexes $(F^{TNpy2})_2Cu^{2+}$ and $(F^{TNpy2})Cu(DMF)^{2+}$ (Scheme S1). The presence of two different species for these stoichiometries is confirmed by the different EPR signatures and parameters extracted from simulations (Figure S10, S12). Finally, Electrochemical studies support these conclusions (Figure S15). The Cu^{II} complexes are characterized by their reduction potentials. Upon titration of F^{TNpy2} in MeCN (Scheme S1), the first species encountered for 0.25 equivalents of Cu^{II} displays a quasi-reversible wave at potential $E_{pc} = -0.57$ V/ $E_{pa} = -0.46$ V. Further addition of Cu^{II} leads to a second quasi-reversible wave at the potential $E_{pc} = -0.29$ V/ $E_{pa} = -0.19$ V, the intensity of which increases with Cu^{II} addition. The latter corresponds to a less donating environment for copper. These species are proposed to be respectively to $(F^{TNpy2})_2Cu^{2+}$ and $F^{TNpy2}Cu(S)^{2+}$, as depicted in the equilibria displayed below. When carried out in MeCN/DMF, these two type of species are observed, but $F^{TNpy2}Cu(S)^{2+}$ ($E_{pc} = -0.48$ V, $E_{pa} = -0.37$ V) is predominant over $(F^{TNpy2})_2Cu^{2+}$ ($E_{pc} = -0.64$ V, $E_{pa} = -0.57$ V) right from the beginning of the titration, which is ascribed to the more donating character of DMF which displaces the equilibrium towards $F^{TNpy2}Cu(S)^{2+}$ (Figure S15).

Upon addition of heptylamine to the $F^{TNpy2}Cu(S)^{2+}$ complex, the reduction wave vanishes from the scanning window in MeCN (tentatively ascribed to hydroxo compounds formation), while it shifts from -0.48 V to -0.57 V in MeCN/DMF, indicating coordination of heptylamine to Cu^{II} in this MeCN/DMF, in agreement with the shift of the Cu^{II} bands in UV-vis spectroscopy from 667 / 867 nm to 639 / 779 nm (Figures S16, S17).

Finally, N-methylimidazole was added to $F^{TNpy2}Cu(S)^{2+}$ in MeCN/DMF in order to mimic the possible coordination of the small rim imidazole groups of the calixarene small rim. The reduction potential shift from -0.48 V to -0.57 V, in agreement with a more donor environment and coordination of Me-Im (Figure S18). Addition of one equivalent of base tetrabutylammonium hydroxide (Figure S18) to this solution leads to a shift of the reduction potential to -0.65 V along with a loss of intensity of the signal. This is ascribed to the formation of a mononuclear hydroxo complex (in the scanning window) in equilibrium with dimers (out of the window).



Scheme S1. Equilibrium between of mononuclear species of F^{TNpy2} .

IV/ Coordination studies on ligand L^{TNpy2}

4.1. EPR studies of the Cu^{II} complexes of ligand L^{TNpy2}

4.1.1. L^{TNpy2} + 3 equiv. Cu^{II} in MeCN/DMF

The spectrum is simulated as the sum of two components in a 3:2 ratio. The major component displays parameters close to those of F^{TNpy2}Cu + 2 MeIm, the minor one to F^{TNpy2}Cu.

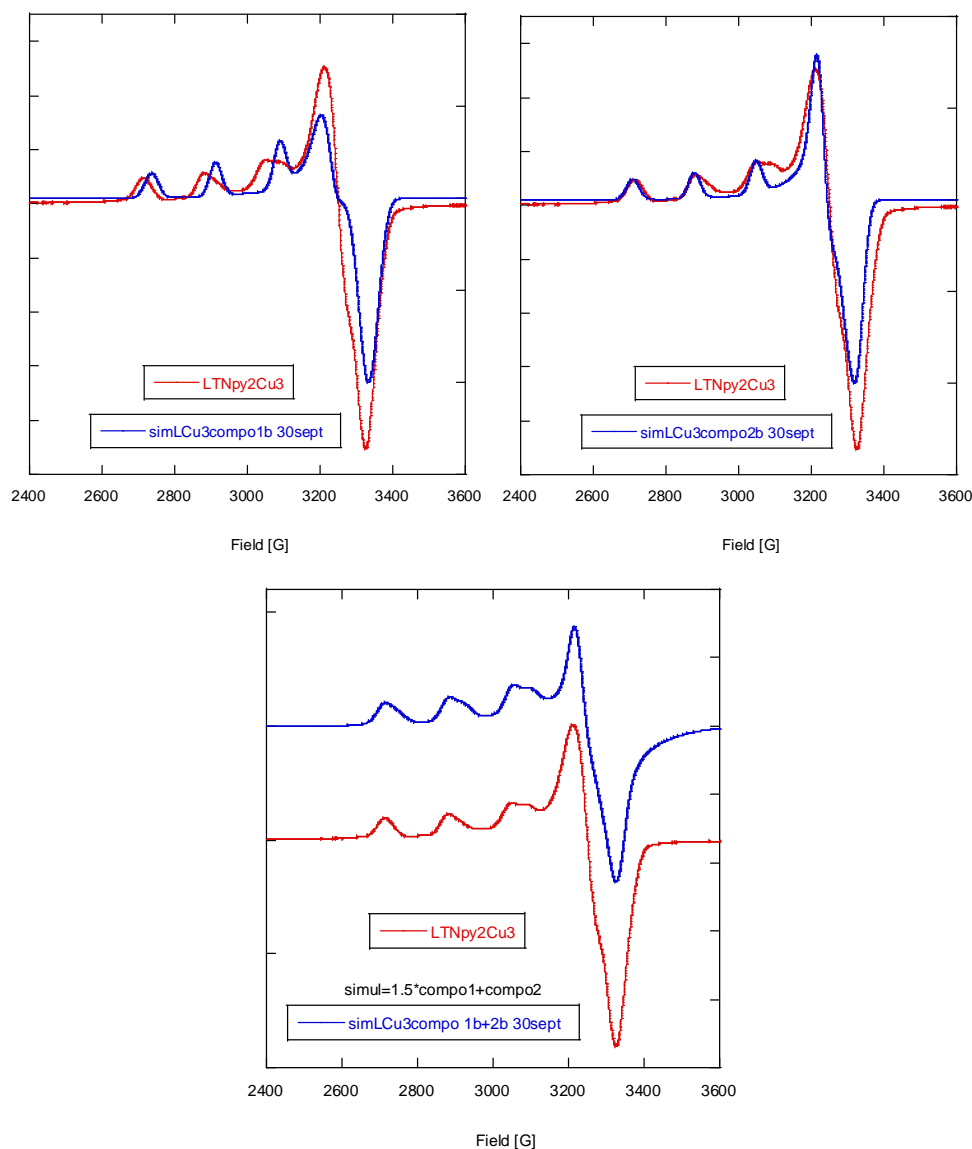


Figure S19. X band EPR spectra (100 K) of L^{TNpy2} + 3 equiv. Cu²⁺ (6 mM in MeCN/DMF 1:1) and corresponding simulation. A_∥ and a_N values in G.

Top: simulation of the isolated components. *Bottom:* Sum of simulated components spectra (1.5 x component 1 + component 2)

L ^{TNpy2} Cu ₃ c1	2.05	2.08	2.235	173	16	16	0
L ^{TNpy2} Cu ₃ c2	2.05	2.08	2.264	168	0	0	0

4.1.2. Addition of heptylamine to a mixture of $L^{\text{TNpy}2}$ and 4 equiv. Cu^{II} in MeCN/DMF

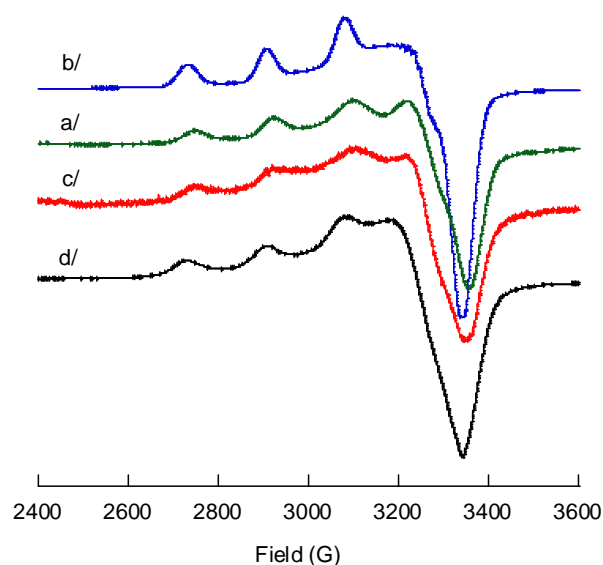


Figure S20. Comparison of the EPR spectrum obtained at the end of the heptylamine titration of a mixture of $L^{\text{TNpy}2}$ and 4 equiv. of Cu^{II} with reference spectra, supporting the binding of the 4th Cu at the small rim upon guest encapsulation: a) $L^{\text{TNpy}2}$ and 4 equiv. of Cu^{II} + 12 equiv. heptylamine; b) $L^{\text{tBu}}\text{Cu}(\text{S})_2^{2+}$ + 6 equiv. heptylamine; c) $F^{\text{TNpy}2}\text{Cu}(\text{S})_2^{2+}$ + 4 equiv. heptylamine; d) free Cu^{2+} + 7 equiv. heptylamine.

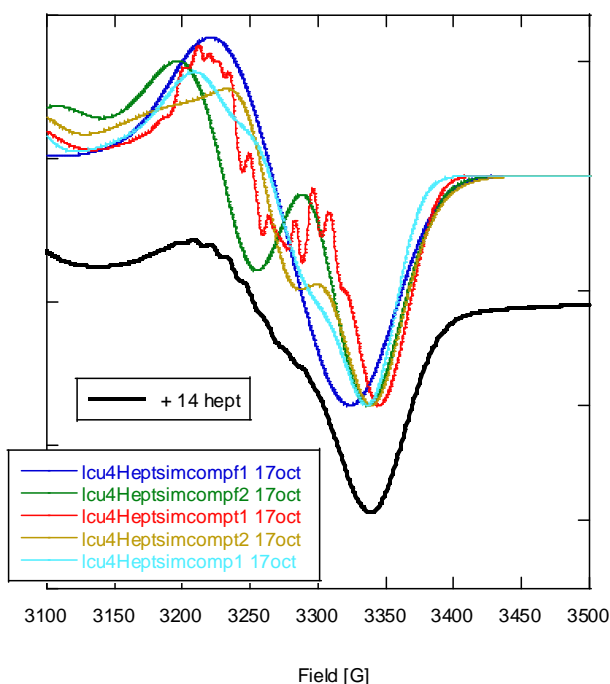
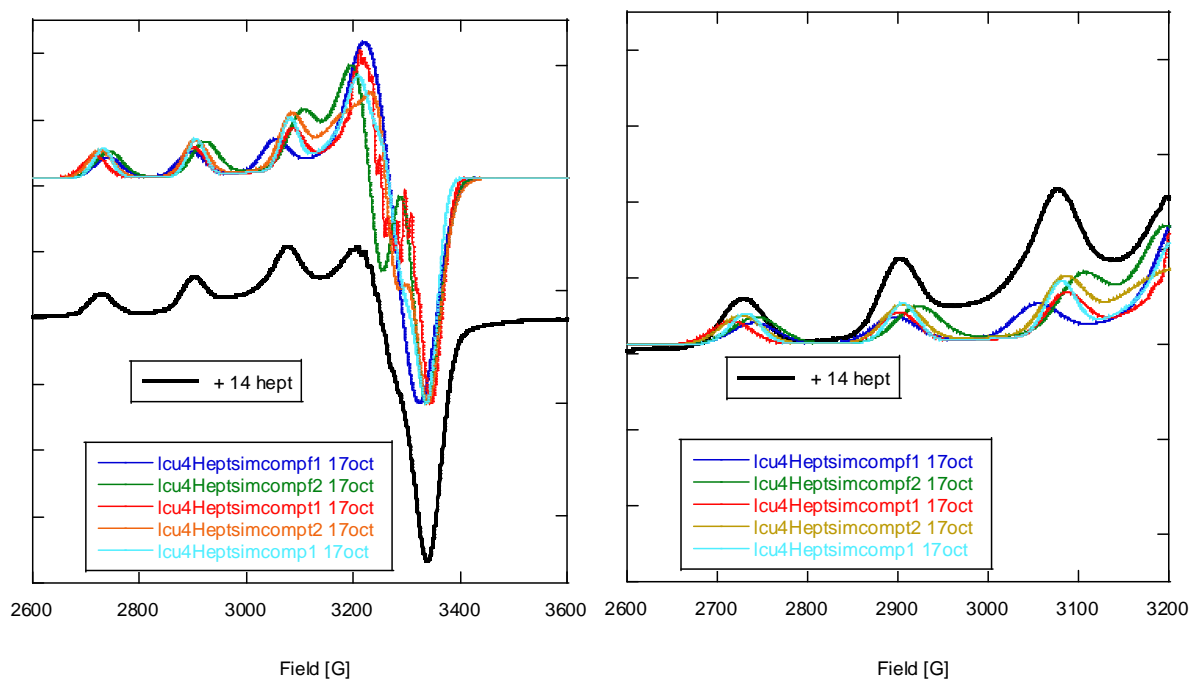


Figure S21. X band EPR spectra (100 K) of L^{TNPY2} (6 mM in MeCN/DMF 1:1) + 4 equiv. Cu^{2+} + 14 equiv. heptylamine (bold black) and various simulations. A_{\parallel} and a_N values in G. Component 1 of the “ $F^{TNPY2}Cu(S)^{2+}$ + 2 equiv. heptylamine simulation (blue), Component 2 of the “ $F^{TNPY2}Cu(S)^{2+}$ + 2 equiv. heptylamine simulation (green), Component 1 of the “ $L^{tBu}Cu(S)_2^{2+}$ + 6 equiv. heptylamine simulation (red), Component 2 of the “ $L^{tBu}Cu(S)_2^{2+}$ + 6 equiv. heptylamine simulation (yellow), “free Cu^{2+} + 6 equiv. heptylamine simulation (light blue). *Top*: simulation of the isolated components. *Bottom*: Sum of simulated components spectra (1.5 x component 1 + component 2)

The experimental spectrum could arise from the superimposition of 3 “ $F^{TNpy2}Cu +$ heptylamine” contributions with either a “ $LtBuCu(S)_2^{2+} + 4$ heptylamine” one or with and “ $freeCu^{2+} + 7$ heptylamine”.

Attempts to sum these contributions in a simulated spectrum does not allow to draw conclusion regarding the location of the fourth Cu ion bound to the TrisIm site or free in solution bound to heptylamine):

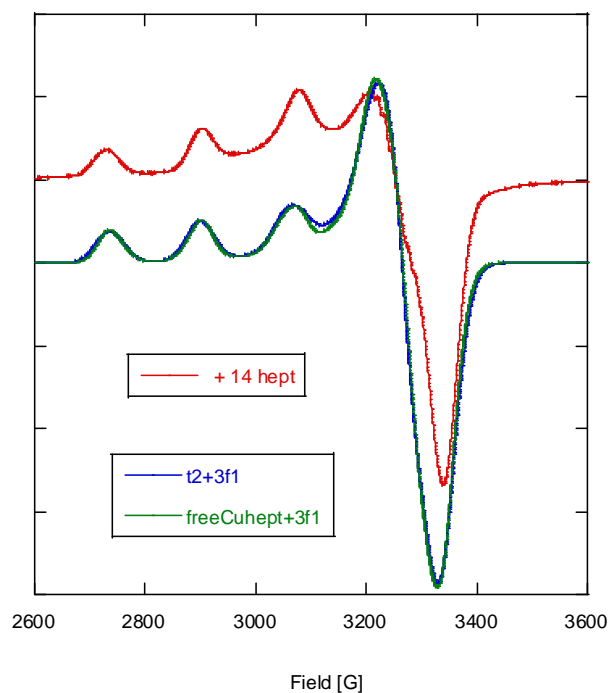


Figure S22. X band EPR spectra (100 K) of L^{TNpy2} (6 mM in MeCN/DMF 1:1) + 4 equiv. $Cu^{2+} + 14$ equiv. heptylamine (red) and various simulations. $A_{//}$ and a_N values in G.

Linear combinations of simulated spectra: t2+3f1 (blue), fc+3f1 (green)
 t2 = Component 2 of the “ $L^{tBu}Cu(S)_2^{2+} + 6$ equiv. heptylamine simulation
 f1 = Component 1 of the “ $F^{TNpy2}Cu(S)_2^{2+} + 2$ equiv. heptylamine simulation
 fc = “free $Cu^{2+} + 6$ equiv. heptylamine simulation

4.2. ^1H NMR coordination and host-guest studies of ligand $L^{\text{TNpy}2}$ towards Zn^{II}

4.2.1. Addition of Zn^{II} to $L^{\text{TNpy}2}$ in CD_3CN

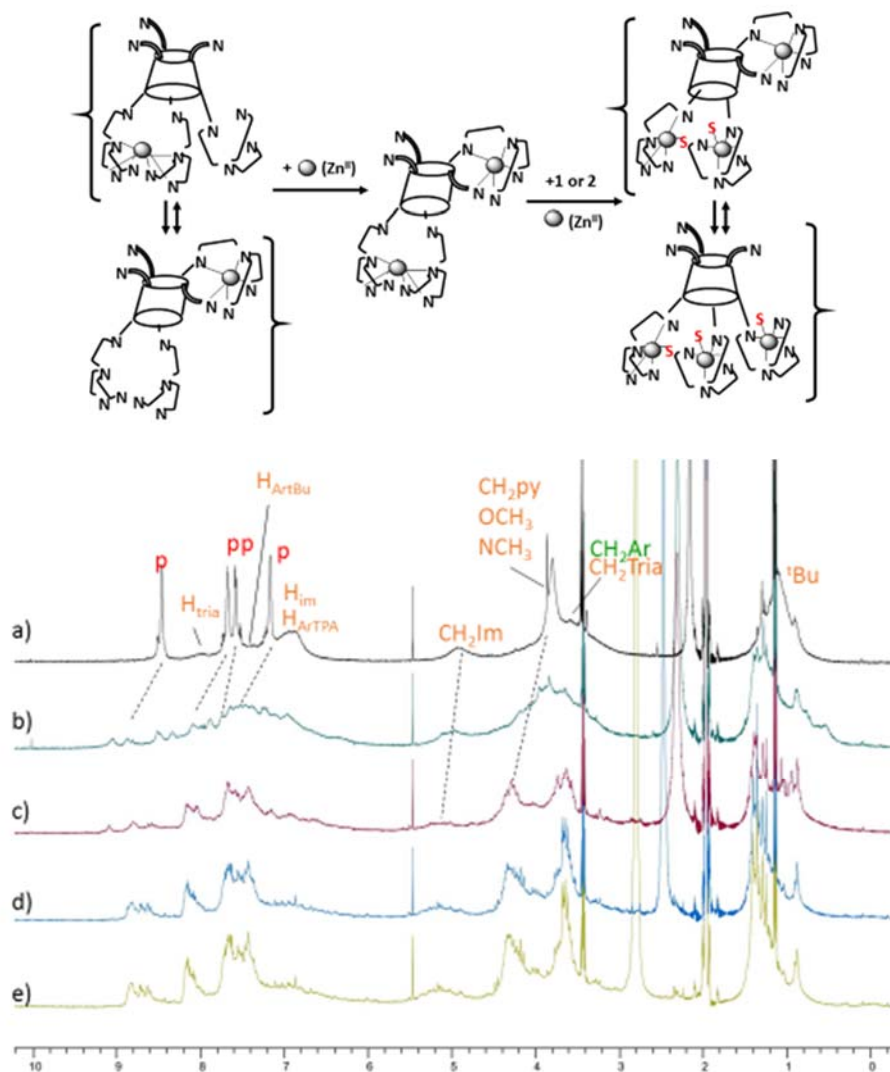


Figure S23. ^1H NMR spectra (CD_3CN , 500 MHz, 300 K) recorded during the titration of $L^{\text{TNpy}2}$ by ZnOTf_2 . a) $L^{\text{TNpy}2}$ (6 mM) + b) 1 equiv. Zn^{II} ; c) 2 equiv. Zn^{II} d) 3 equiv. Zn^{II} e) 4 equiv. Zn^{II} .

The spectrum of $L^{\text{TNpy}2}$ displays broad resonances (due to the conformational motion of the calixarene on the NMR timescale), except for the pyridyl ones that remain sharp due to their higher mobility.

Upon addition of one equivalent of Zn^{II} (Figure S23, a and b), the pyridyl and CH_2py resonances are downfield shifted, indicating Zn^{II} coordination at the $\text{F}^{\text{TNpy}2}$ -like sites. The ortho pyridyl proton resonances (initially at 8.47 ppm) split into three peaks, one correspond to the unbound state (8.47 ppm, ascribed to a pendant tetradentate group) and the other two (8.88 and 9.05 ppm) correspond to Zn^{II} bound states with different environments. The CH_2Im resonances are also slightly downfield shifted, indicating their (partial) coordination (likely in

a $F^{TNpy_2}Zn(Im)$ environment). But the overall unsymmetrical spectrum that is obtained discards a small rim “Tris-Im” coordination which would lead to a more symmetrical spectrum (especially in the H_{Bu} region: a single peak should be expected). The distribution of species depicted above can thus be proposed.

Upon addition of the second equivalent of Zn^{II} (Figure S23 b and c), the ortho pyridyl resonances corresponding the unbound state (8.47 ppm) are downfield shifted, indicating the coordination of the dangling tetradentate group. The structure depicted above can be proposed.

For three equivalents of Zn^{II} (Figure S23 c and d), the pyridyl resonances almost merge, which indicate a similar binding mode for all three Zn^{II} complexes, as depicted above. Furthermore, the spectrum ceased to evolve after 3 equivalents of Zn^{II} (Figure S23 d and e), suggesting the 4th Zn^{II} ion remains free in solution.

4.2.

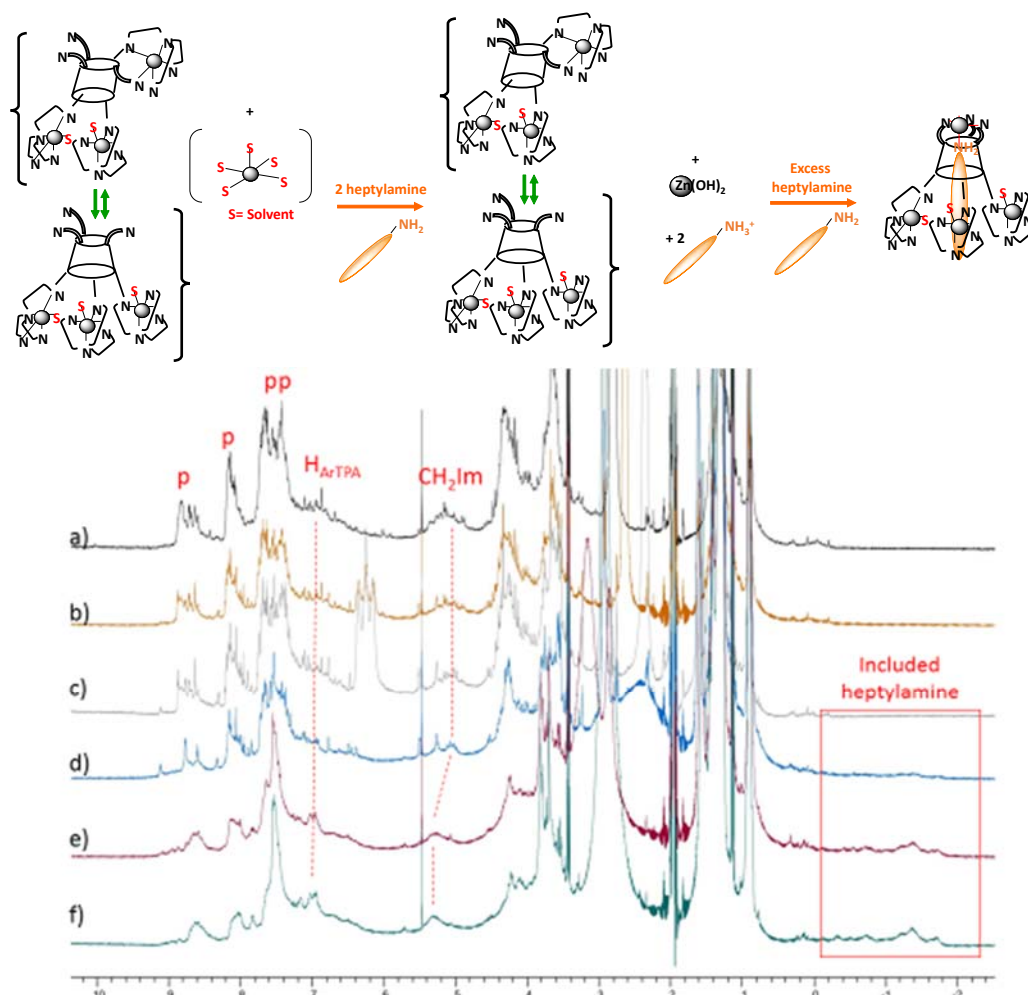


Figure S24. 1H NMR spectra (CD_3CN , 500 MHz, 300 K) recorded during the titration of L^{TNpy_2} / Zn^{II} 1:4 by heptylamine. a) L^{TNpy_2} / Zn^{II} 1:4 (6 mM) + b) 1 equiv. heptylamine; c) 3 equiv. heptylamine; d) 5 equiv. heptylamine; e) 7 equiv. heptylamine; f) 10 equiv. heptylamine.

Upon addition of heptylamine to the $L^{\text{TNpy}2} / \text{Zn}^{\text{II}}$ 1:4 mixture (Figure S24), a signal appears at 6.3 ppm for the first 3 equivalents and disappears afterwards: This is typical of an ammonium group, in agreement with heptylamine initially reacting with free Zn^{II} to form the hydroxide. Further addition of heptylamine leads to a simplification of the spectrum indicating a more symmetrical species, along with a downfield shift of the CH_2Im resonances, typical of amine binding at the small rim. This last point is confirmed by the resonances that appears between 0 and -2 ppm, which are the signature of heptylamine encapsulated within the cone-shaped calixarene cavity and anchored to the small rim Zn^{II} . Indeed, the CH_2 groups of the amine chain sit in the shielding cones of the aromatic walls of the cavity. This behavior is in agreement with the 4th Zn^{II} being initially converted to $\text{Zn}(\text{OH})_2$ by the basic amine and for further addition of guest, rebound to the small rim Tris-Im site with concomitant encapsulation of guest. Heptylamine stabilizes Zn at the small rim due to the strength of the coordination bond, secondary H-bonds developing between the N-H bonds of the bound guest and the crown of O atom of the small rim, and finally CH- π interactions between the guest chain and the aromatic walls of the calixarene.

VI Titrations of free Cu^{2+} by heptylamine

5.1. EPR studies of free Cu^{2+} in the presence of heptylamine

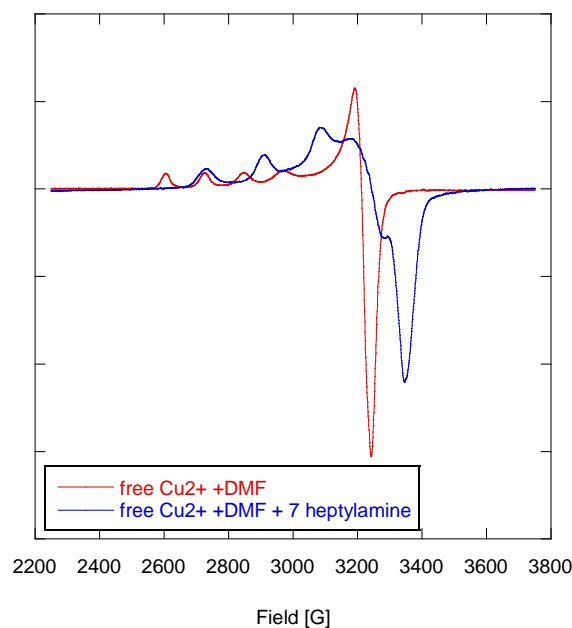


Figure S25. X-band EPR spectrum (100 K) of free $\text{Cu}(\text{OTf})_2$ in MeCN/DMF before (black) and after addition of 7 equiv. of heptylamine (blue). Corresponding double integrated signals (right).

5.2. UV-vis studies of free Cu^{2+} in the presence of heptylamine

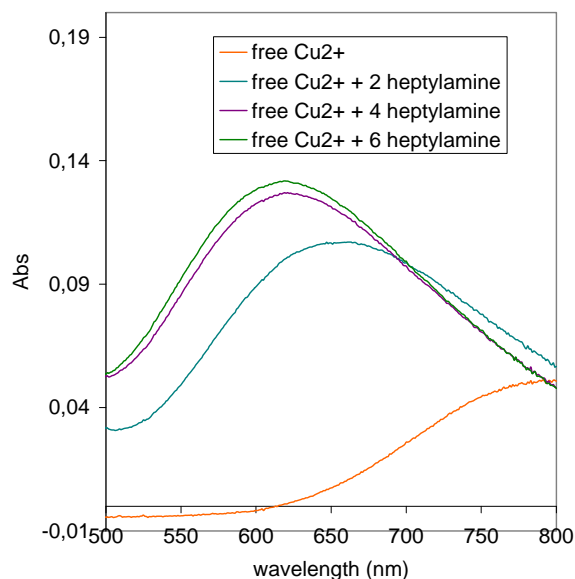


Figure S26. UV-vis spectrum (293 K, 1 mM) of free $\text{Cu}(\text{OTf})_2$ in MeCN/DMF before and after addition of increasing equivalents of heptylamine. Addition of heptylamine to free Cu^{II} in MeCN/DMF, leads to a maximum shift from 800 to 650 nm (first equivalents) and then 600 nm

5.3. Electrochemical studies of free Cu^{2+} in the presence of heptylamine

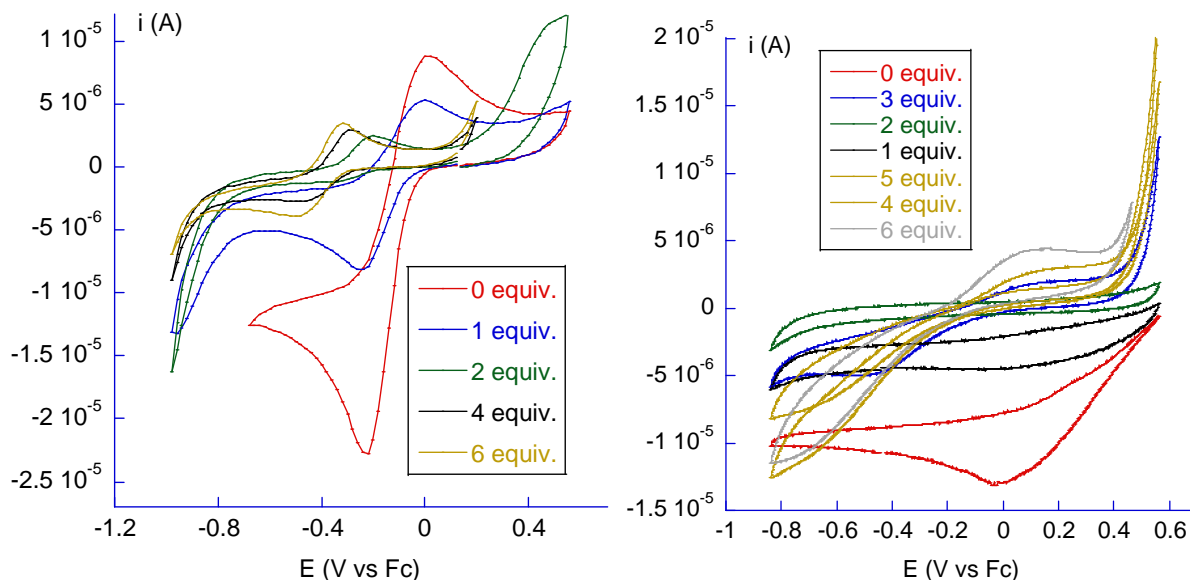


Figure S27. CVs at GC electrode (E/V vs Fc, $v = 0.1 \text{ V/s}$, NBu_4PF_6 0.1 M) recorded upon addition of heptylamine to free Cu^{2+} . *Left*: in MeCN/DMF, ClO_4^- salt. *Right*: in MeCN, OTf^- salt. Solutions were scanned in reduction to the lowest possible potential to discard the appearance of a redissolution peak in oxidation.

5.4. ESI-MS studies of the polynuclear L^{TNPpy2}/Cu^{2+} systems

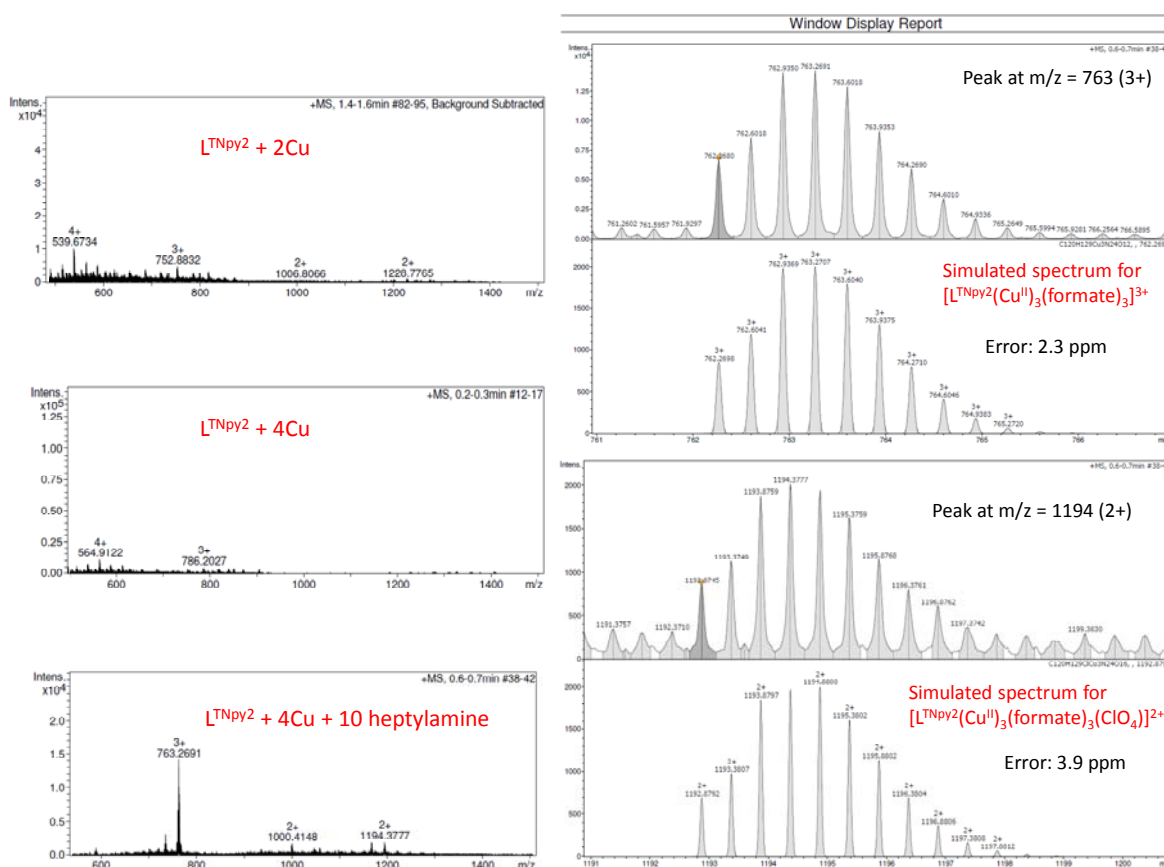


Figure S28. ESI-MS spectra (DMF/MeCN) of solutions obtained from mixtures of “ L^{TNPpy2} and 2 equiv. Cu^{II} ”, “ L^{TNPpy2} and 4 equiv. Cu^{II} ” and “ L^{TNPpy2} , 2 equiv. Cu^{II} and 10 equiv. heptylamine” (Left). No significant peaks can be detected in the absence of heptylamine. However when 10 equivalents of heptylamine are added to the ESI-MS-silent “ $L^{TNPpy2} + 4Cu$ ” solution, a clear peak appeared at $m/z = 762.2680$ ($3+$). Simulated spectra of the peak at $m/z = 762.2680$ ($3+$) ascribed to the polynuclear species $[L^{TNPpy2}(Cu^{II})_3(formate)_3]^{3+}$ (calculated 762.2698, error 2.3 ppm) and the peak at $m/z = 1192.8745$ ($2+$) ascribed to $[L^{TNPpy2}(Cu^{II})_3(formate)_3(ClO_4)]^{2+}$ (calculated 1192.8792, error 3.9 ppm) (Right). The guest-dependent presence of the peaks suggests that a different species (host-guest adduct) with different ionization properties forms in solution upon addition of the guest. The fourth copper ion, weakly bound, is lost upon ionization.

(1) Colasson, B.; Save, M.; Milko, P.; Roithova, J.; Schroder, D.; Reinaud, O. *Org. Lett.* **2007**, *9*, 4987.

- (2) Bernier, N.; Menard, N.; Colasson, B.; Rebilly, J.-N.; Reinaud, O. *Inorg. Chem.* **2013**, *52*, 4683.
- (3) Huang, S.; Clark, R. J.; Zhu, L. *Org. Lett.* **2007**, *9*, 4999.